TSINGHUA SCIENCE AND TECHNOLOGY
ISSN 1007-0214 04/16 pp481–494
DOI: 10.26599/TST.2021.9010044
Volume 27, Number 3, June 2022

Overview of Ultra-Wideband Transceivers—System Architectures and Applications

Bowen Wang, Haixin Song, Woogeun Rhee*, and Zhihua Wang

Abstract: The Ultra-WideBand (UWB) technique, which offers good energy efficiency, flexible data rate, and high ranging accuracy, has recently been recognized as a revived wireless technology for short distance communication. This paper presents a brief overview of two UWB techniques, covering Impulse-Radio UWB (IR-UWB) and Frequency-Modulation UWB (FM-UWB) methods. The link margin enhancement technique, Very-WideBand (VWB), and power consumption reducing technique, chirp UWB, are also introduced. Then, several potential applications of IR-UWB with transceiver architectures are addressed, including high data rate proximity communication and secure wireless connectivity. With fine-ranging and energy-efficient communication features, the UWB wireless technology is highly promising for secure mobile Internet of Things (IoT) applications.

Key words: Ultra-WideBand (UWB); Impulse Radio UWB (IR-UWB); Frequency-Modulation UWB (FM-UWB); Very-WideBand (VWB); transceivers; wireless security; mobile Internet of Things (IoT)

1 Introduction

As wireless markets for mobile connectivity and Internet of Things (IoT) grow, short distance communication has become an important area in modern wireless systems. Existing narrowband wireless standards, e.g., Bluetooth Low Energy (BLE), Wireless Fidelity (WiFi), and Zig-Bee, share the Industrial Scientific Medical (ISM) band, and have difficulty in meeting the demand of next-generation mobile connectivity systems. The BLE and Zig-Bee techniques dramatically reduce system complexity and power consumption. However, they suffer from a limited data rate below 2 Mb/s. Recent WiFi systems can achieve a data rate of up to several Gb/s, but the complex system design significantly increases power consumption. Moreover, processing latency becomes a serious problem.

On the other hand, the Ultra-WideBand (UWB) not only offers a flexible data rate with high energy efficiency, but also features fine ranging capability, which is highly promising for secure mobile connectivity. The Federal Communication Commission (FCC) defines the UWB signal by one of two conditions[1]: (1) The signal bandwidth should be wider than 0.2 times carrier frequency; or (2) the signal bandwidth should be wider than 500 MHz. To avoid interfering with other narrow bandwidth communication, the Power Spectral Density (PSD) of the UWB signal should be lower than -41.3 dBm for the noise integration bandwidth of 1 MHz, i.e., –41.3 dBm/MHz. The typical PSD of the UWB signal is shown with the spectrum mask in Fig. 1.

For UWB transmissions, two techniques are mainly proposed. One is Impulse-Radio UWB (IR-UWB), and the other is Frequency-Modulation UWB (FM-UWB).

In the IR-UWB system, various modulation methods, such as Binary Phase Modulation (BPM), On-Off-Keying (OOK), Pulse Amplitude Modulation (PAM), Pulse Width Modulation (PWM), and Pulse Position Modulation (PPM), can be employed. A narrow high-order Gaussian pulse is applied to modulate a Radio-Frequency (RF) signal, achieving an ultra-wide

• Bowen Wang, Haixin Song, Woogeun Rhee, and Zhihua Wang are with the School of Integrated Circuits, Tsinghua University, Beijing 100084, China. E-mail: wbw18@mails.tsinghua.edu.cn; shx19920918@sina.com; wrhee@tsinghua.edu.cn; zhihua@tsinghua.edu.cn.
* To whom correspondence should be addressed.
Manuscript received: 2021-03-01; revised: 2021-06-29; accepted: 2021-07-02

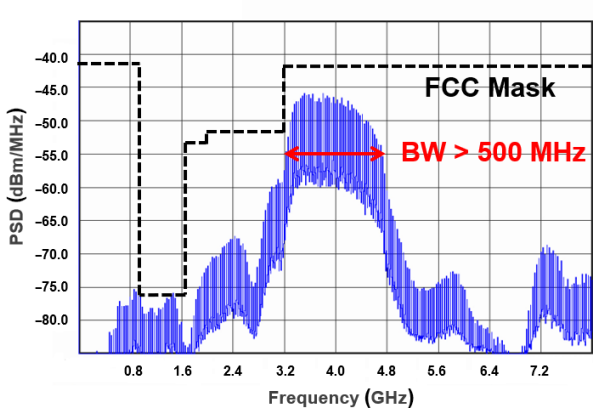

Fig. 1 Typical UWB signal PSD[2].

spectrum[2, 3]. Since the pulse width is very narrow and the duty cycle is as low as 1%, the UWB pulse can provide high resolution in time and space. Thus, the IR-UWB technique can be applied to ranging applications with high accuracy[4]. The low duty cycle of the UWB pulse makes the transceiver significantly reduce power consumption with intermittent operation[5]. Thanks to high-ranging accuracy and low-power operation features, the IR-UWB technique has received greater attention than ever for mobile IoT applications. However, synchronization between a transmitter and a receiver is very challenging due to the low duty-cycled operation[6]. Moreover, a pulse with a large peak voltage is needed to increase bit energy, making it difficult to increase communication distance, especially when a low-voltage transceiver design is considered[7]. To solve the problems of synchronization and high peak voltage, a frequency-hopping based transmission method was proposed, which is called Very-WideBand (VWB).

Unlike the IR-UWB system, the FM-UWB system generates a constant-envelope UWB signal, featuring a flat in-band PSD and a steep spectral roll-off[8–10]. The principle of the FM-UWB technique is based on the double frequency modulation method[8]. This method can be divided into two steps. The first step is that baseband data are transferred to an analog triangle waveform with frequencies f_1 and f_2 through Binary Frequency Shift Keying (BFSK) modulation, which is called subcarrier generation. The second step is that the triangle waveform is sent to the control voltage of a Voltage-Controlled Oscillator (VCO). The output frequency of the VCO is modulated by a wide-range control voltage, generating a wideband FM spectrum. This step is called RF modulation. Since the FM-UWB has a constant envelope and does not create a high peak voltage, it is more suitable for low-voltage CMOS design. However, the FM-UWB has several critical disadvantages. Firstly, RF front-end blocks cannot perform a low power duty-cycled operation, since the FM-UWB has a continuous waveform. Accordingly, energy efficiency is much worse than that of the IR-UWB. To further improve the energy efficiency of the FM-UWB transceiver, a chirp UWB technique based on intermittent FM modulation is proposed[11]. Secondly, it is difficult to achieve a high data rate since a short modulation period reduces the FM modulation index that is set by the ratio of the peak deviation frequency to the modulation frequency.

Table 1 shows the comparation between the IR-UWB and the FM-UWB. Benefiting from the fine-ranging and energy-efficient communication features, the IR-UWB has a more promising future for secure mobile IoT applications.

In this paper, the basic system architectures and applications of the UWB technique are introduced. The paper is organized as follows. In Section 2, the basic UWB system is overviewed. Section 3 shows UWB applications with the example of system implementation, followed by conclusion in Section 4.

2 Overview of UWB System

2.1 Impulse radio UWB

(1) Signal characteristic

The IR-UWB obtains a very narrow duration pulse. The center frequency f_c and the bandwidth BW of the IR-UWB signal are related with a pulse waveform in the time domain. To improve spectrum efficiency, the pulse envelope should be shaped to satisfy the strict constraints. The UWB signal with pulse shaping features a steep spectral roll-off, so as to obtain good spectrum efficiency. Institute of Electrical and Electronics Engineers (IEEE) defines the UWB reference pulse $r(t)$ as a root raised

Table 1 Comparation between IR-UWB and FM-UWB.

Type	IR-UWB	FM-UWB
Signal	Short-duration pulse	Wideband FM
Energy efficiency	Better	Worse
Sensitivity	Worse	Better
Enhanced transmission	VWB (for link margin)	Chirp UWB (for energy efficiency)
Application	Low data rate, high data rate, fine ranging	Low data rate

cosine pulse with a roll-off factor of $\beta = 0.5$[12],

$$r(t) = \frac{4\beta}{\pi\sqrt{T_p}} \frac{\cos\left[\frac{(1+\beta)\pi t}{T_p}\right] + \frac{\sin\left[\frac{(1-\beta)\pi t}{T_p}\right]}{4\beta\left(\frac{t}{T_p}\right)}}{1-\left(\frac{4\beta t}{T_p}\right)^2},$$

where the pulse duration T_p differs from different channels, and the typical value is 2 ns for most channels. The real UWB pulse $p(t)$ should be similar to the reference pulse $r(t)$. Normalized cross-correlation between two waveforms is applied to evaluate the similarity, which is defined by

$$\phi(\tau) = \frac{1}{\sqrt{E_r E_p}} \mathrm{Re}\left(\int_{-\infty}^{\infty} r(t)p^*(t+\tau)\mathrm{d}t\right),$$

where E_r and E_p are the energies of $r(t)$ and $p(t)$, respectively. The first constraint is that the peak value of a main lobe should be greater than 0.8. The second constraint is that the peak value of sidelobes should be less than 0.3. To satisfy the strict constraint, some pulse-shaping techniques need to be employed, as shown in Fig. 2, which will be further introduced in the next chapter.

(2) Basic system architecture

The IR-UWB system architecture is simple. The transmitter can be sorted by the pulse-shaping circuit, which is the most important block in the IR-UWB transmitter. There are three kinds of pulse shaping transmitters, the analog, digital, and hybrid pulse shaping transmitters.

Figure 3 shows the block diagram of an analog pulse shaping transmitter[13]. To satisfy the spectrum mask, a shaped Gaussian pulse is generated by an analog Low Pass Filter (LPF). Then, the pulse is mixed with a Local Oscillating (LO) signal, producing an RF signal. Passive devices in the LPF occupy a large area and cannot be scaled down with advanced CMOS technology.

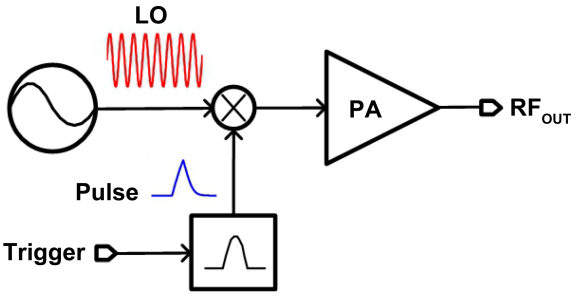

Fig. 3 Block diagram of analog pulse shaping transmitter.

Recently, a digital pulse shaping technique becomes popular[14–16]. It is compatible with the digital process and can offer good technology scalability. In addition, static power can be reduced with the duty-cycled operation. The digital pulse shaping technique can be divided into two parts; one is with multiple Digital Power Amplifiers (DPAs), and the other is with a single DPA. The block diagram of a digital pulse-shaping transmitter with multiple DPAs is shown in Fig. 4a[15]. It consists of a delay line, NOR gates, and DPAs. The delay line forms a time interval with high resolution. Multi-phase pulses are generated by the DPAs in parallel. The parasitic capacitors of the parallel antenna drivers limit the signal bandwidth. The main disadvantage of this architecture is that the multiple PAs occupy a large area. For that reason, a digital pulse shaping method with a single DPA is proposed. Figure 4b shows a transmitter architecture with a single binary-weighted DPA[16]. In this architecture, high-speed digital blocks are employed, which offers a digital-intensive design with a compact area, but causes the problem of reduced energy efficiency.

Accordingly, a hybrid pulse shaping technique that does not rely on high-speed digital blocks is proposed[17], as shown in Fig. 5. Transistors in parallel generate a digital envelop waveform that is mixed with an LO signal. By replacing the high-speed digital blocks with parallel transistors, the hybrid architecture can achieve a data

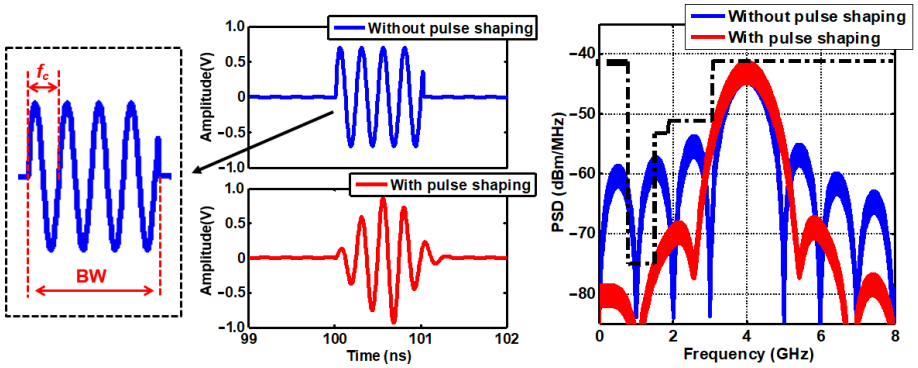

Fig. 2 Function of pulse shaping.

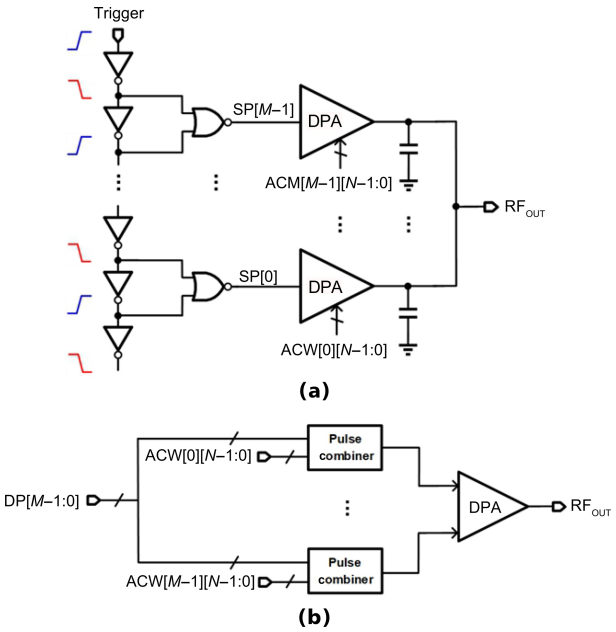

Fig. 4 Block diagram of digital pulse shaping transmitter: (a) with multiple DPAs and (b) with a single DPA.

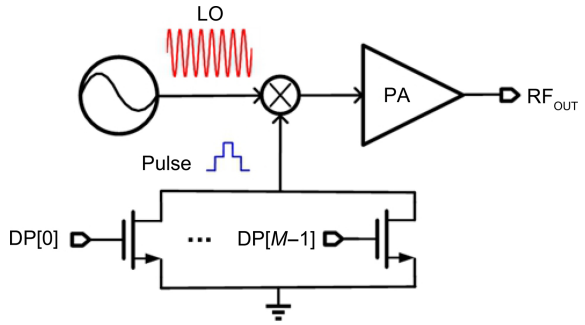

Fig. 5 Block diagram of hybrid pulse shaping transmitter.

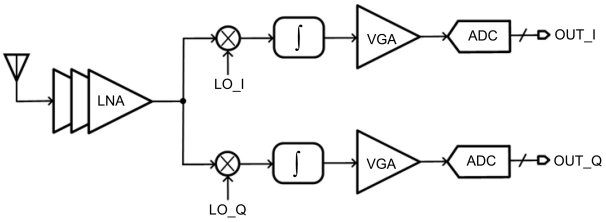

Fig. 6 Block diagram of IR-UWB coherent receiver.

rate of up to 2 Gb/s with reasonable power consumption.

Similar to the conventional narrowband receiver, the UWB receiver has two types of architectures, that is, the coherent receiver[18, 19] and the noncoherent receiver[20]. The block diagram of the coherent receiver is shown in Fig. 6. Compared with the noncoherent receiver, the coherent receiver not only achieves better sensitivity, but also provides better immunity against NarrowBand Interference (NBI). However, the coherent receiver requires a synchronized LO signal, requiring a high-performance Phase-Locked Loop (PLL). Because of the settling time problem of the PLL, it is difficult to implement a duty-cycled operation for the coherent receiver. In the noncoherent receiver, as shown in Fig. 7, an RF signal is down-converted through self-mixing. Not requiring an LO signal, the noncoherent receiver has better energy efficiency than the coherent receiver. The performance of the noncoherent receiver, however, is significantly degraded when the NBI is present.

(3) Enhanced link margin technique

Based on the FCC's regulation, the IR-UWB transmitting power density should not exceed –41.3 dBm/MHz. With the spectrum efficiency η, and the –10 dB bandwidth $\mathrm{BW}_{-10\,\mathrm{dB}}$, the TX output power P_{TX} should satisfy

$$P_{\mathrm{TX}} \leqslant (-41.3\,\mathrm{dBm/MHz}) \cdot \mathrm{BW}_{-10\,\mathrm{dB}} \cdot \eta.$$

For the 500 MHz bandwidth, the maximum transmitting power is –15.86 dBm. Besides, considering from the energy of each pulse and the Pulse Repetition Frequency (PRF), the output power P_{TX} can be rewritten as

$$P_{\mathrm{TX}} = E_{\mathrm{S,\,RF}} \cdot \mathrm{PRF} = \frac{(V_{\mathrm{RF}}/\sqrt{2})^2}{R} \cdot \frac{b}{\sqrt{2}} \cdot \mathrm{PRF},$$

where $E_{\mathrm{S,\,RF}}$ represents the energy of each pulse, and b represents the pulse width when the pulse amplitude is 0.5 times the maximum amplitude. If we assume that the antenna characteristic impedance R is 50 Ω, we can derive the relationship between the maximum pulse amplitude $V_{\mathrm{RF,\,MAX}}$ and PRF when the signal bandwidth is 500 MHz.

From Fig. 8, it is easy to find that the $V_{\mathrm{RF,\,MAX}}$ increases to keep the same transmitting power when the PRF decreases in the IR-UWB transceiver. When

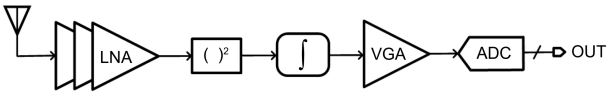

Fig. 7 Block diagram of IR-UWB noncoherent receiver.

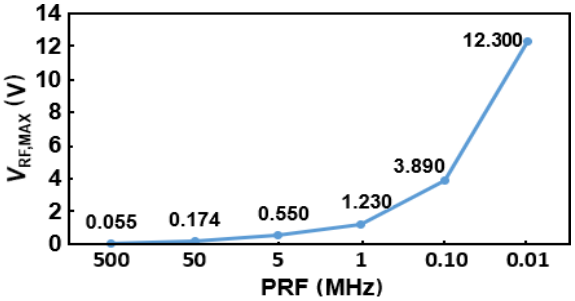

Fig. 8 Relationship between $V_{\mathrm{RF,\,MAX}}$ and PRF.

the PRF decreases to 1 MHz, $V_{\mathrm{RF,MAX}}$ becomes 1.23 V. Moreover, when the PRF further decreases to 100 kHz, $V_{\mathrm{RF,MAX}}$ increases up to 3.89 V, far exceeding the supply voltage. One possible solution is to send several redundant bits in one symbol period. However, it mitigates the advantage of intermittent operation for power saving in the design of an IR-UWB transceiver.

To overcome the limited pulse energy for low-voltage applications, a novel transmission method based on a Frequency-Hopping (FH) sinusoidal OOK pulses is proposed[7] and termed VWB, as individual pulses do not have to exceed 500 MHz spectral occupancy. Therefore, the VWB transmission offers a more flexible link margin control over different data rates and distances for the given power budget than the UWB transmission.

Figure 9 shows a simplified block diagram of a VWB transmitter and the comparison of the VWB and the IR-UWB signals in time and frequency domains.

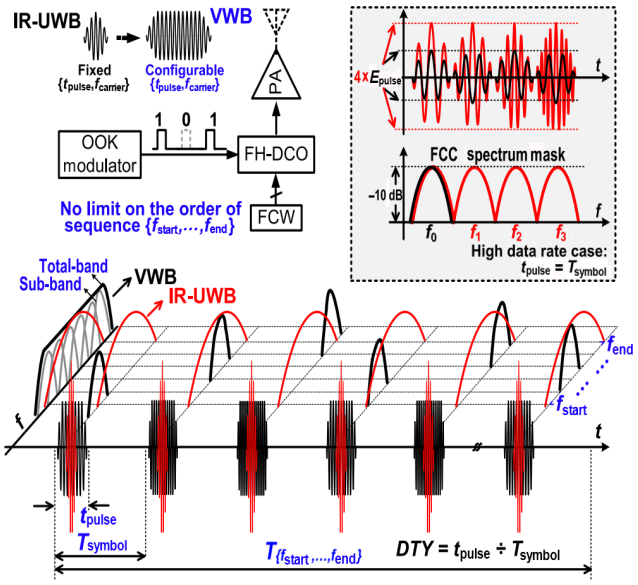

Fig. 9 VWB transmission for enhanced link margin, where DCO is Digital-Controlled Oscillator.

In the design of the transmitter, the pulse generation circuit design is significantly relaxed without requiring very narrow pulse width generation and complex pulse-shaping function. In the receiver, the synchronization process can be relaxed with much longer pulse duration. Different from the conventional FH spread spectrum, the FH rate is the same as the PRF in the VWB technique. Thanks to the FH feature, the signal bandwidth can achieve 500 MHz by spreading the output spectrum to satisfy the UWB spectrum mask.

Since each pulse does not necessarily have >500 MHz bandwidth, the power density increment and the pulse duration determine the required number of subbands. As shown in Fig. 10, by choosing different numbers of the FH subbands, the different data-rate signal can achieve the same maximum pulse amplitude and duty cycle without increasing the peak power P_{TX}. Besides, the VWB technique provides better spectrum roll-off characteristic. As the number of the subbands increases, the bandwidth of combined subbands becomes narrow, and the overall output spectrum exhibits steeper spectral roll-off.

2.2 FM-UWB

(1) Signal characteristic

Compared to the IR-UWB, the FM-UWB generates a constant-envelope UWB signal with wideband frequency modulation. The signal features an ultra wideband with a flat in-band PSD and a steep spectral roll-off. As described previously, the signal generation of the FM-UWB signal is based on the double frequency modulation. The modulation procedure contains two steps. The first one is sub-carrier generation, where the subcarrier generator transforms baseband data to an analog triangle waveform with double frequencies, f_1 and f_2, by using BFSK modulation. And the second one is the RF modulation, where the sub-carrier is used to

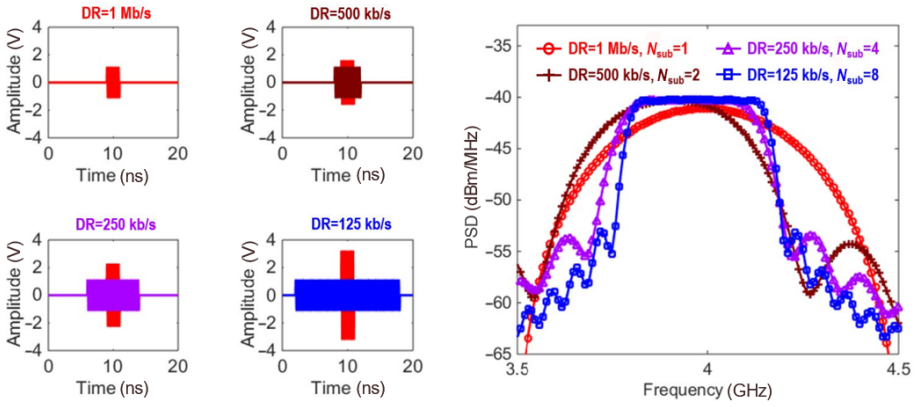

Fig. 10 VWB spectrum with different data-rates and subbands.

modulate the RF signal. Different kinds of sub-carrier waveforms decide the RF signal characteristic, as shown in Fig. 11. The ideal triangular sub-carrier obtains a flat in-band PSD. Otherwise, the ideal sinewave sub-carrier obtains a steep spectral roll-off. Thanks to the wide bandwidth, the FM-UWB has a good sensitivity and is relatively insensitive to NBI. However, the constant envelope is not available to the duty-cycled operation, which reduces the system energy efficency.

(2) System architecture

Figure 12 shows the simplified block diagram of an FM-UWB transmitter consisting of a sub-carrier generator and an RF modulator.

There are two ways of achieving the sub-carrier generation. The first one is based on the Direct-Digital Frequency Synthesizer (DDFS)[21]. The other one is based on the fractional-N PLL[9]. The DDFS-based method completes data processing and sub-carrier generation in the digital domain. A Digital-to-Analog Converter (DAC) directly converts a digital signal to an analog signal. To generate an accurate sub-carrier, the DDFS requires high resolution, resulting in high power consumption. Accordingly, the sub-carrier generation based on the fractional-N PLL is considered a viable solution for low-power design. A block diagram is shown in Fig. 13. The fractional-N PLL consists of a PFD, a Charge Pump (CP), a LooP Filter (LPF), a VCO, a Multi-Modulus Divider (MMD), and a Delta-Sigma Modulator (DSM). The binary data modulate the MMD through the DSM, achieving BFSK modulation.

The RF frequency modulator consists of a high-gain open-loop VCO and a Center Frequency Calibration Block (CFCB)[10], as shown in Fig. 14. The sub-carrier serves as the control voltage of the open-loop VCO. Under the control of amplitude-frequency conversion of the VCO, a linearly increased or decreased triangle waveform is converted to a constant envelope FM-UWB signal. Since the open-loop VCO is sensitive to the Process, Voltage, and Temperature (PVT) variations, the CFCB is introduced to suppress the center frequency drift. The common topology of the CFCB is a Frequency Locked Loop (FLL). Even though the instantaneous VCO output frequency changes quickly

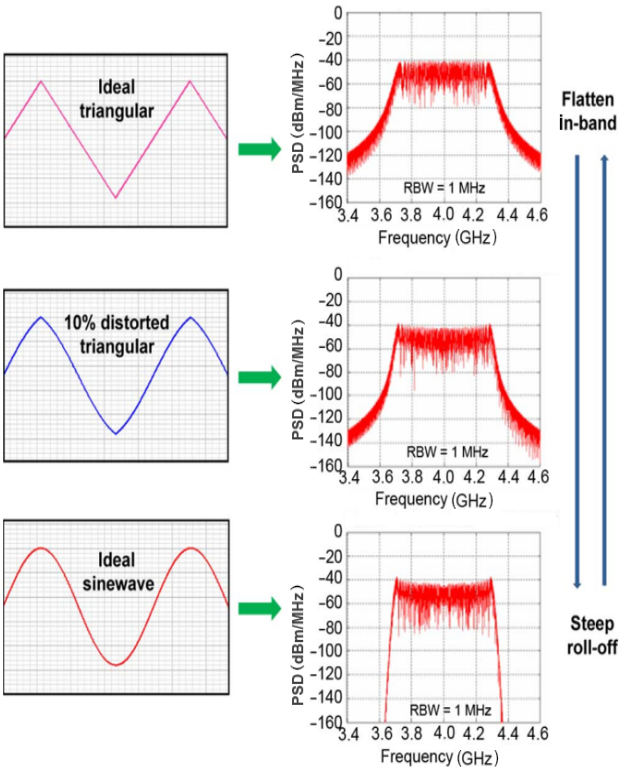

Fig. 11 Relationship between sub-carrier waveforms and RF signal characteristic.

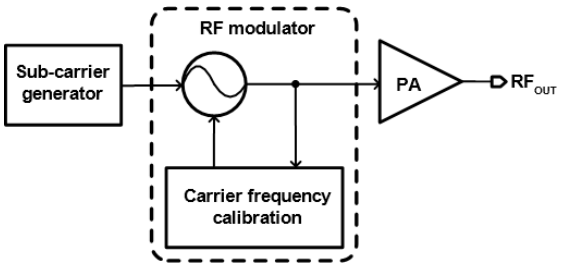

Fig. 12 Block diagram of FM-UWB transmitter.

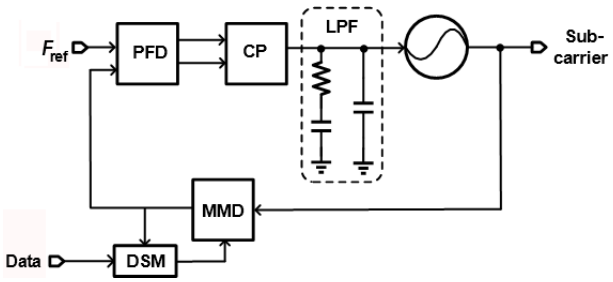

Fig. 13 Block diagram of PLL based subcarrier generation.

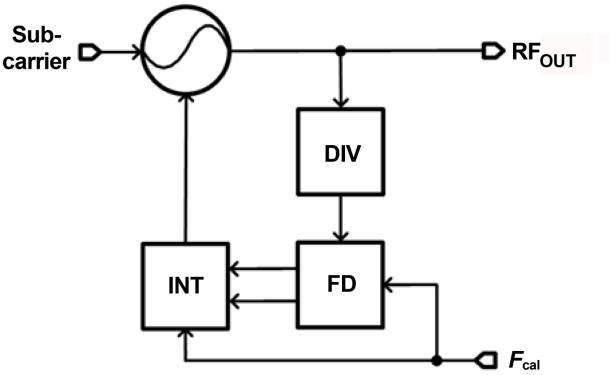

Fig. 14 Block diagram of RF frequency modulator.

due to modulation, the average frequency and the center frequency do not change much. Therefore, a narrow-bandwidth FLL is used to calibrate the center frequency of the VCO. A Frequency Detector (FD) detects the center frequency deviation by counting clock periods and controls the subsequent integrator (INT). The VCO modulation is performed by an open-loop path for a fast response, while the calibration loop has a slow response with the closed-loop operation. As a result, the center frequency calibration does not affect the modulation performance of the VCO.

To demodulate a wideband FM signal, two common methods can be considered; slope-frequency detection[22] and phase-frequency detection[23]. In the slope detection method, an FM signal is converted to an AM-FM signal, the envelope of which represents the modulation signal. Then, demodulation information can be obtained by using an envelope detector in the following stage. In the phase-frequency detection method, the FM signal is converted to a PM-FM signal whose phase information can be demodulated by a phase detector. After the RF demodulation, the FSK sub-carrier can be demodulated by using a common coherent FSK demodulation method[21]. Since the sub-carrier is not a high-frequency signal, the system power consumption is mainly determined by the RF demodulation. Moreover, serving as the first stage, the system noise performance also depends on the RF demodulation. Therefore, we only focus on the RF demodulation in this paper.

The slope-frequency detector consists of a BandPass Filter (BPF) and an envelope detector. Figure 15 shows a dual BPFs based demodulator[24]. The center frequencies of the two BPFs are symmetric. The FM-UWB signal is mapped to a voltage signal by the BPFs and demodulated by the following envelope detector. Compared with a single BPF based demodulator, the dual BPFs based demodulator not only suppresses a DC

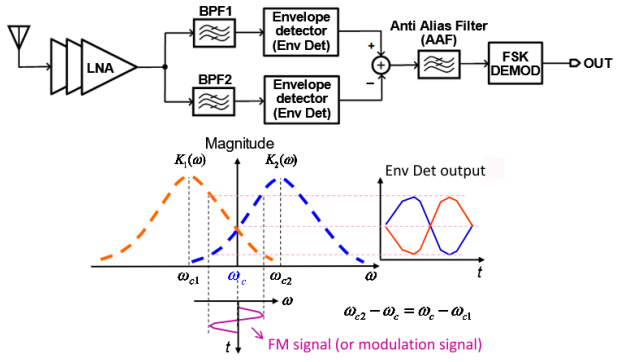

Fig. 15 Dual BPFs based demodulator.

offset introduced by the NBI, but also exhibits good linearity or small distortion, resulting in an enhanced demodulation quality. To minimize the variation of the BPFs center frequencies over PVT variations, a binary-weighted capacitor array can be designed for frequency calibration.

The phase-frequency detection block consists of a delay line and a multiplier, as shown in Fig. 16. Suppose that the RF FM signal V_{FM} is given by

$$V_{\mathrm{FM}} = A \cdot \cos[(\omega_c + k\Omega(t))t + \phi_0],$$

where A represents the RF signal amplitude, ϕ_0 represents the original phase, and k represents the frequency-modulation coefficient. Then, a PM signal V_{PM} after the delay line is expressed as

$$V_{\mathrm{PM}} = A \cdot \cos[(\omega_c + k\Omega(t))(t-\tau) + \phi_0] = A \cdot \cos[(\omega_c + k\Omega(t))t - (\omega_c + k\Omega(t))\tau + \phi_0],$$

where τ represents the delay time. The sub-carrier signal V_{sub} can be recovered after the multiplier and an AAF, that is,

$$V_{\mathrm{sub}} = G \cdot V_{\mathrm{FM}} \cdot V_{\mathrm{PM}} = 0.5G \cdot A^2 \cdot \cos[(\omega_c + k\Omega(t))\tau = 0.5 \cdot G \cdot A^2 \sin[k\Omega(t)\tau] \approx 0.5 \cdot G \cdot A^2 k\Omega(t)\tau \propto \Omega(t),$$

where G represents the multiplier gain. The delay time should be $N/(4f_c)$ to ensure a good FM-PM conversion. To achieve high-resolution and tunable delay time, a Current-Mode-Logic (CML) delay line is commonly used. The delay line based demodulator is relatively insensitive to PVT variations because of the turntable delay time. However, it is quite challenging to design a high-resolution delay line with small power consumption.

(3) Power consumption reduction technique

To overcome the lack of duty-cycled operation in the FM-UWB, the chirp UWB technique was proposed[11]. The chirp UWB obtains a low duty cycle, such as 10%, for each pulse. In each pulse, the FM-UWB based wideband frequency modulation method is applied. For example, a reducing chirp represents "0" and an increasing chirp represents "1", as shown in Fig. 17. The chirp UWB inherits the advantages of the IR-UWB and the FM-UWB. On one hand, an only 10% duty cycle helps to reduce the power consumption as compared to

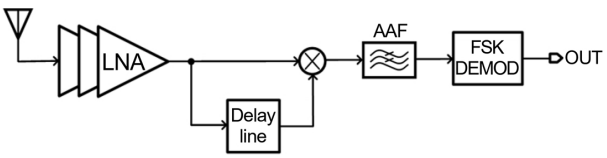

Fig. 16 Block diagram of phase frequency detector.

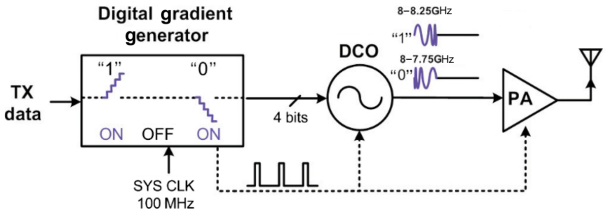

Fig. 17 Block diagram of chirp UWB transmitter.

the FM-UWB. On the other hand, the 10% duty cycle is much wider than the duty cycle in the IR-UWB. As a result, it inherits the advantages of the FM-UWB, which not only reduces the peak transmission power to achieve the same link margin but also relaxes the difficulty in the baseband synchronization. However, the chirp UWB increases the system design complexity, especially for the transmitter. A high-speed digital gradient generator is needed, which makes the high data rate communication unachievable.

3 Application Example

The FM-UWB is proposed for low power communication, such as the medical application. Recently, the power consumption of the narrowband communication system is dramatically reduced. Therefore, the FM-UWB has no obvious advantage over the narrowband communication system. However, the IR-UWB, featuring a narrow duration pulse width, has two equal applications, which cannot be replaced by the narrowband communication. The first one is energy-efficient high data rate communication[25–29]. As shown in Table 2, the narrowband communication systems, such as BLE and WiFi, can only achieve a low or medium data rate. Though the 5th generation New Radio (5G NR) based on millimeter Wave (mm-Wave) can achieve a high data rate, it focuses on the long distance application with ultra high power consumption. As a result, the IR-UWB has been recognized as a good solution for energy-efficient high data rate communication with relatively short distance. And the second application is the fine-ranging based secure communication[30–32]. The narrow duration pulse obtains a high time resolution. As a result, the IR-UWB is promising for the RF distance bounding protocol. Based on the two unique applications, the IR-UWB has been recognized as a revived wireless technology for short distance communication.

Table 2 Comparation between different communication systems.

Communication system	Data rate	Range	Power
BLE	Low	Short	Low
WiFi	Medium	Medium	Medium
mm-Wave	High	Long	High
IR-UWB	High	Short	Low

3.1 High data rate communication

The mm-Wave radio exhibits great potential in high speed communication with an ample unlicensed spectrum for use, but it suffers from a high peak DC power to achieve an acceptable link margin. On the contrary, the pulse-based UWB transceiver achieves a much better link margin and energy efficiency with low frequency band and reduced hardware complexity. Moreover, it enables an asymmetric architecture with a low-power transmitter and a high performance receiver. Figure 18 shows an example of a high data rate proximity communication for smartphone-mirrored display systems. Even though the proximity connectivity is a near-range point-to-point communication, the multipath fading effect is still critical for the Gb/s transmission, especially when a noncoherent wideband receiver is employed. Hence, a phase-array receiver can be implemented in the display equipment to achieve robust communication with good directivity.

Figure 19 shows the block diagram of a 2 Gb/s UWB proximity transmitter with 7.6 mW power

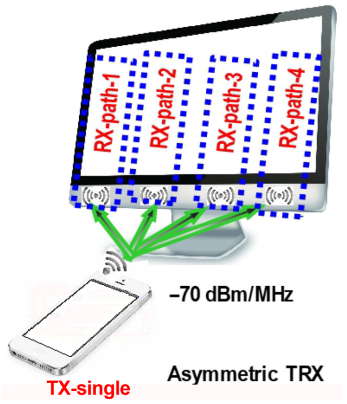

Fig. 18 Smartphone-mirrored display system.

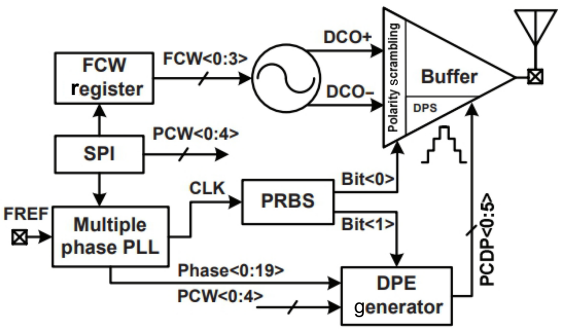

Fig. 19 Block diagram of a high data rate transmitter.

consumption[17]. In the transmitter, the hybrid pulse shaping architecture is used to reduce the power consumption and design complexity as shown in Fig. 20a. To achieve the high data rate, a pre-correction method for Inter-Symbol Interference (ISI) is proposed as shown in Fig. 20b. The bit stream data are delayed by one clock period, so that the data can be detected before the Digital Pulse Envelope (DPE) generation. When the data change from "1" to "0", the multiplexer will change to choose the pre-configured reconstruction digital phases $P^*<0:5>$ instead of the original one $P<0:5>$, which can effectively suppress the ISI. The transmitter is fabricated in 65 nm CMOS. Thanks to the wide bandwidth and the simple architecture, the transmitter achieves up to 2 Gb/s data rate with 7.6 mW power consummation at 8 GHz, in which 2.3 mW is consumed by the 2 GHz PLL and 2.1 mW is consumed by the output buffer. The output power density of –70 dBm/MHz easily meets the UWB masks of most countries and is enough for proximity communication within a distance of a few centimeters.

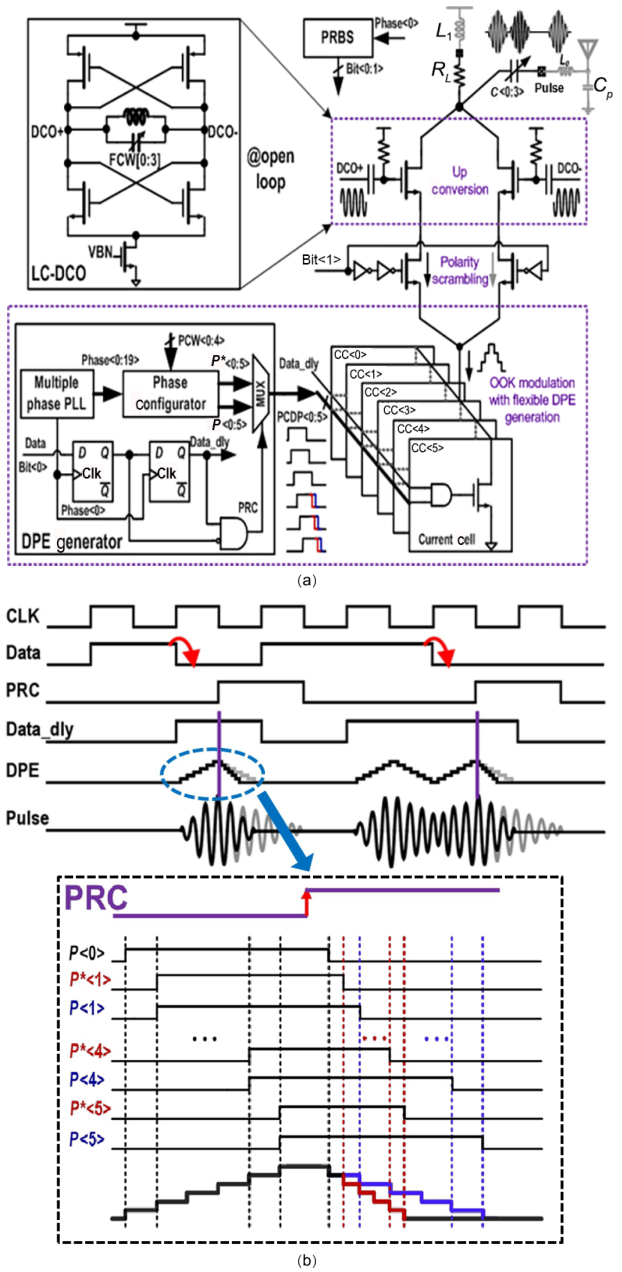

Fig. 20 Details of a high data rate transmitter: (a) hybrid pulse shaping architecture and (b) ISI pre-correction method.

Figure 21 shows the block diagram of a dual-antenna UWB receiver for proximity communications[25]. The receiver is based on the noncoherent architecture with energy detection to reduce the power consumption and system complexity. The Auto Beam Steering (ABS) scheme is applied to the receiver. The phase rotator is automatically adjusted to align the phase of two incoming pulses received from the two antennas, which acquires the maximum baseband signal. By performing the signal superposition in the RF domain, it improves the sensitivity up to 6 dB with good directivity, which exceeds the 3 dB improvement in the conventional coherent receiver performing the signal superposition in the digital domain. Thanks to the around 8 GHz UWB band, the phase rotator does not significantly increase the power consumption compared to the phase rotator in the mm-Wave receiver. The receiver is implemented in 65 nm CMOS process, occupying 1.8 mm×1.5 mm. The transceiver can achieve 1 Gb/s data rate with 31.8 mW power consumption with the sensitivity of –54.4 dBm.

3.2 Secure communication with fine ranging

Secure communication becomes essential for IoT

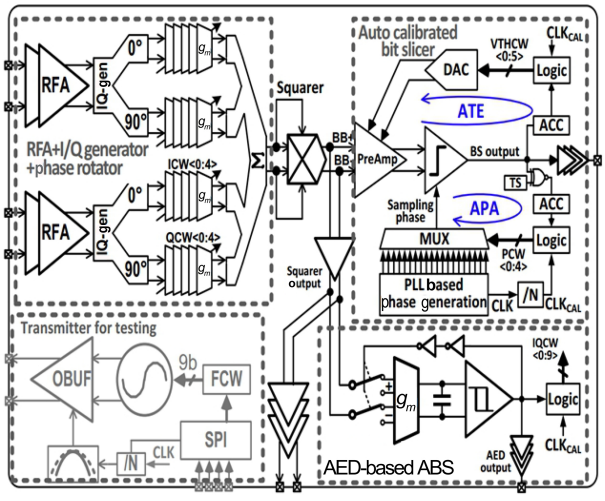

Fig. 21 Block diagram of a high data rate receiver.

and mobile authentication applications. The narrow bandwidth communication technologies, such as WLAN and BLE, can easily achieve a low power transceiver design. However, the public key encryption dramatically increases the hardware complexity, latency, and power consumption. Besides, without reliable location information, the wireless authentication is not secure enough because of the relay-attack problem, as shown in Fig. 22. If the prover and the verifier are far away from each other, two attackers, A_1 and A_2, who are close to prover and verifier, respectively, are able to relay messages between two legal entities. These two entities can gain access to the verifier without decrypting the actual data being transmitted. The UWB technique has been recognized as one of the candidates to prevent the relay attacks, which is promising in secure communicating application. There are two benefits making the UWB technique be immune to the rely attacks. Firstly, the UWB transceiver can simultaneously achieve communication and ranging functions. If the distance between a transmitter and a receiver can be measured, secure wireless transmission can be achieved based on the distance-bounding protocol. In Fig. 22, when prover and verifier exchange verification information, the distance-bounding protocol limits the maximum distance $d_{\max}$ between the prover and the verifier based on the Time-of-Fight (ToF) measurement. Secondly, the UWB signal can be demodulated by the envelope detection based noncoherent receiver with a short processing latency. Showing in Fig. 22, as $d_{\max}$ is limited by the distance-bounding protocol, the distance advantage Δd for attackers is brought about by the processing latency. As a result, having a low processing latency is critical for the secure communication. Compared to the narrow band communication techniques, the UWB signal can be demodulated within several nanoseconds, which reduce the attacking distance to less than 1 m.

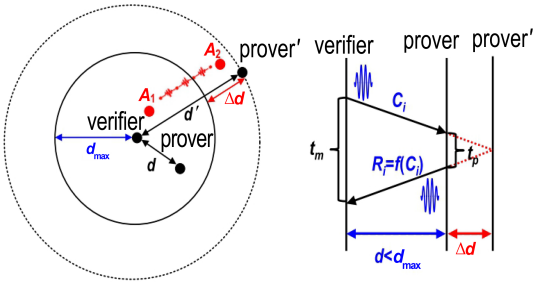

Fig. 22 Relay attack problem and distance-bounding protocol.

As the ranging accuracy is vital to the secure wireless communication. The ΔΣ energy detection was proposed to achieve fine ranging[30]. Figure 23 shows a noncoherent receiver with the ΔΣ energy detector. The receiver can achieve PPM demodulation and ΔΣ energy detection based ranging. The basic concept of the ΔΣ energy detection is shown in Fig. 24. It can be divided into two steps. The first step is synchronization and coarse ranging as illustrated in Fig. 24a. The energy integration block integrates the energy from a received pulse in a short time window. Then, the output is quantized by a 7-bit Successive-AppRoximation Analog-to-Digital Converter (SAR ADC). While the integration window is moving with the step τ_p, the quantized output is also changing. By searching the maximum integrated energy, an optimum integration window WIN_{i+1} can be determined for fine ranging. The second step is the ΔΣ energy detection based fine ranging, as shown in Fig. 24b. In this step, the optimized integration window WIN_{i+1} is divided into two parts, WINP and WINN. The energy integration block chooses one of the integration windows according to the digital output D_{OUT}, and integrates the energy from a received pulse to the reversed direction. After a complete integration, the average value of the digital output represents the accurate position of the received pulse between the rising edge and the falling edge of WIN_{i+1}.

Besides, the 2-bit modulation method is proposed for low processing latency encrypted communication between the verifier and the prover. The UWB transceiver can simultaneously contain two modulation methods, such as PPM and PWM. As a result, one symbol period signal contains 2-bit information. Figure 25 shows the basic concept of the 2-bit modulation[31]. Initially, the verifier sends C_i to modulate the position of the pulse. The Envelope-Detection (ED) based noncoherent prover receives the pulse, and the PWM is immediately triggered by the

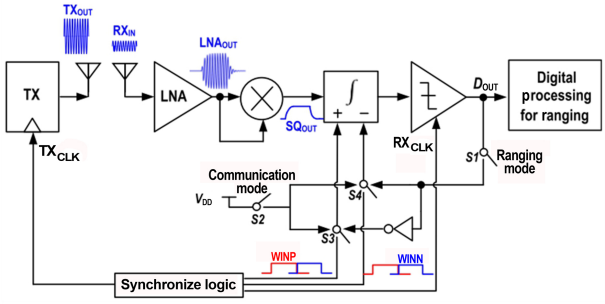

Fig. 23 Noncoherent receiver with ΔΣ energy detector.

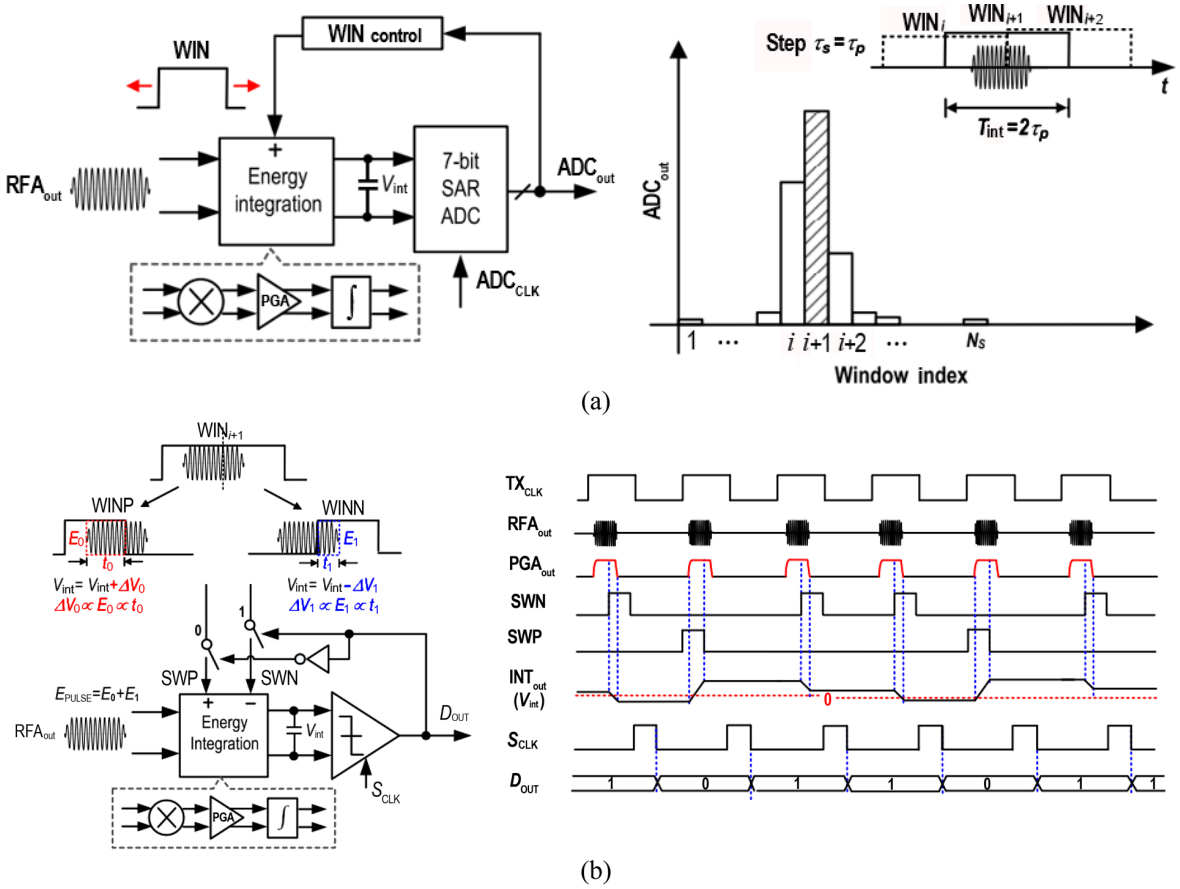

Fig. 24 Basic concept of ΔΣ energy detection: (a) synchronization and coarse ranging and (b) ΔΣ energy detection based fine ranging.

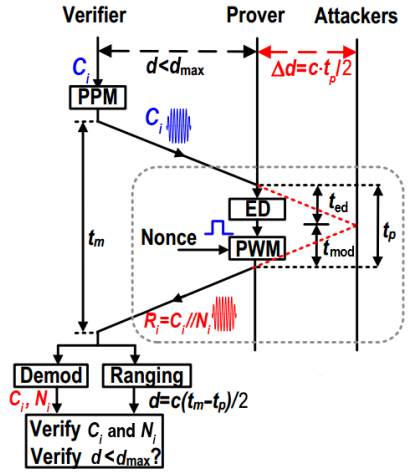

Fig. 25 Basic concept of 2-bit modulation.

rising edge of the received pulse, which dramatically reduces the processing latency. The prover nonce N_i is also modulated into the UWB signal. Thus, the verifier can obtain 2-bit information within one symbol period. Moreover, the transmitter and the receiver have the FH feature based on a secret key, which further increases the communication security.

The transceiver is implemented in 65 nm CMOS. Figure 26a shows the ΔΣ energy detection based ranging performance with 10 ns pulse width. The transceiver can achieve 2 cm ranging accuracy within a 1.5 m distance. Figure 26b shows the testing result of 2-bit modulation. The verifier sends the PPM signal $\mathrm{RFA_{out}}$, which contains the information C_i. The prover receives the PPM signal, and adds 1-bit information N_i to produce the response pulse, which is modulated by the PWM. The transceiver achieves –80 dBm sensitivity when the data rate is scaled to 1 Mb/s with 8.3 mW power consumption. Experimental results show that the UWB technology is highly promising for mobile authentications and IoT applications with low power and fine ranging features.

4 Conclusion

With the features of low power consumption, flexible date rate, and fine ranging, the UWB technique has been revived as one of the key technologies for next-generation wireless connectivity. Two main UWB techniques are discussed in this paper. The IR-UWB

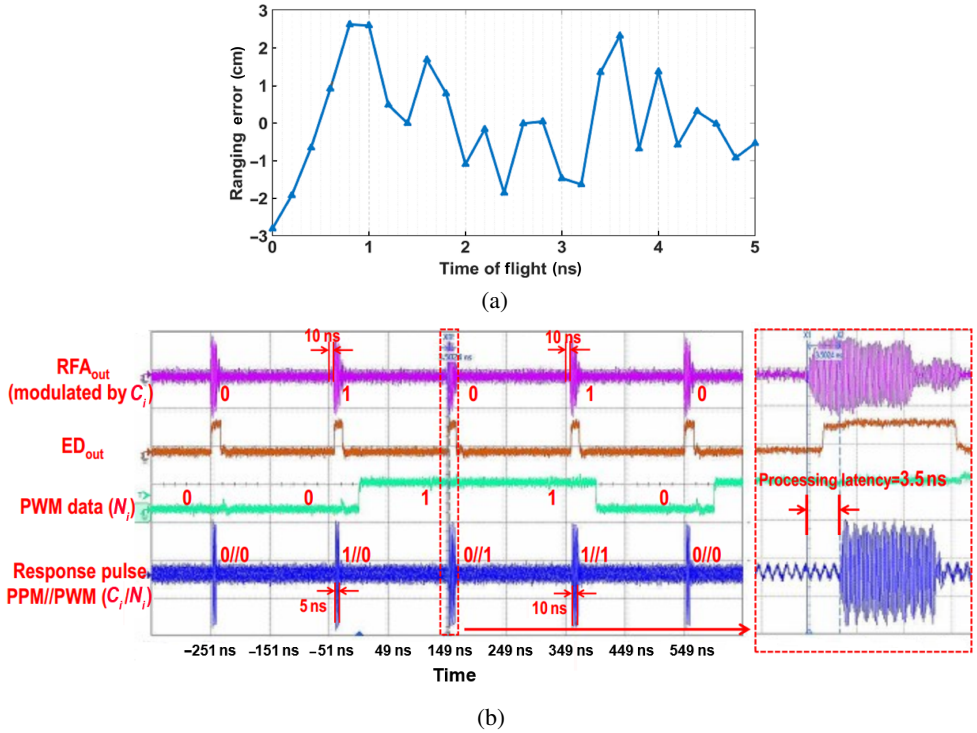

Fig. 26 Testing results of the fine ranging based secure communication transceiver: (a) ΔΣ energy detection based ranging performance and (b) 2-bit modulation transient waveform.

has a simple architecture with good energy efficiency. In addition, benefiting from the short duration pulse, the IR-UWB has a high time resolution. The FM-UWB is based on the wideband frequency modulation, which aims to achieve a low power communication with an enhanced link margin. Unfortunately, with the improvement of narrowband communication, the advantage of the FM-UWB is not evident. On the contrary, thanks to the two unique applications, the energy-efficient high data rate communication and the fine-ranging based secure communication, the IR-UWB is showing a promising future for secure IoT applications.

Acknowledgment

This work was supported in part by the National Natural Science Foundation of China (No. 61774092).

References

[1] L. Q. Yang and G. B. Giannakis, Ultra-wideband communications: An idea whose time has come, *IEEE Signal Process. Mag.*, vol. 21, no. 6, pp. 26–54, 2004.

[2] S. L. Geng, X. C. Chen, W. Rhee, J. Kim, D. Kim, and Z. H. Wang, A power-efficient all-digital IR-UWB transmitter with configurable pulse shaping by utilizing a digital amplitude modulation technique, in *Proc. 2012 IEEE Asian Solid State Circuits Conf.* (*A-SSCC*), Kobe, Japan, 2012, pp. 85–88.

[3] S. L. Geng, W. Rhee, and Z. H. Wang, A pulse-shaped power amplifier with dynamic bias switching for IR-UWB transmitters, in *Proc. 2012 IEEE Int. Symp. Circuits and Systems* (*ISCAS*), Seoul, Republic of Korea, 2012, pp. 2529–2532.

[4] Q. Shi, S. Zhao, X. Cui, M. Lu, and M. Jia, Anchor self-localization algorithm based on UWB ranging and inertial measurements, *Tsinghua Science and Technology*, vol. 24, no. 6, pp. 728–737, 2019.

[5] T. Terada, R. Fujiwara, G. Ono, T. Norimatsu, T. Nakagawa, M. Miyazaki, K. Suzuki, K. Yano, A. Maeki, Y. Ogata, et al., Intermittent operation control scheme for reducing power consumption of UWB-IR receiver, *IEEE J. Solid-St. Circ.*, vol. 44, no. 10, pp. 2702–2710, 2009.

[6] M. U. Nair, Y. J. Zheng, C. W. Ang, Y. Lian, X. J. Yuan, and C. H. Heng, A low SIR impulse-UWB transceiver utilizing chirp FSK in 0.18 μm CMOS, *IEEE J. Solid-St. Circ.*, vol. 45, no. 11, pp. 2388–2403, 2010.

[7] D. Liu, X. W. Ni, R. R. Zhou, W. Rhee, and Z. H. Wang, A 0.42-mW 1-Mb/s 3- to 4-GHz transceiver in 0.18-μm CMOS with flexible efficiency, bandwidth, and distance control for IoT applications, *IEEE J. Solid-St. Circ.*, vol. 52, no. 6, pp. 1479–1494, 2017.

[8] J. F. M. Gerrits, M. H. L. Kouwenhoven, P. R. van der Meer, J. R. Farserotu, and J. R. Long, Principles and limitations of ultra-wideband FM communications systems, *EURASIP J. Adv. Signal Process.*, vol. 2005, p. 189150, 2005.

[9] B. Zhou, R. He, J. Qiao, J. H. Liu, W. Rhee, and Z. H. Wang, A low data rate FM-UWB transmitter with-based sub-carrier modulation and quasi-continuous frequency-locked loop, in *Proc. 2010 IEEE Asian Solid-State*

Circuits Conf., Beijing, China, 2010, pp. 1–4.

[10] B. Zhou, H. Lv, M. Wang, J. H. Liu, W. Rhee, Y. M. Li, D. Kim, and Z. H. Wang, A 1 Mb/s 3.2–4.4 GHz reconfigurable FM-UWB transmitter in 0.18 μm CMOS, in *Proc. 2011 IEEE Radio Frequency Integrated Circuits Symp.*, Baltimore, MD, USA, 2011, pp. 1–4.

[11] F. Chen, Y. Li, D. Liu, W. Rhee, J. Kim, D. Kim, and Z. H. Wang, A 1 mW 1 Mb/s 7.75-to-8.25 GHz chirp-UWB transceiver with low peak-power transmission and fast synchronization capability, in *Proc. 2014 IEEE Int. Solid-State Circuits Conf. Digest of Technical Papers* (*ISSCC*), San Francisco, CA, USA, 2014, pp. 162–163.

[12] IEEE standard for low-rate wireless networks, https://ieeexplore.ieee.org/document/9144691, 2020.

[13] X. Wang, Y. Yu, B. Busze, and H. W. Pflug, A meter-range UWB transceiver chipset for around-the-head audio streaming, in *Proc. 2010 IEEE Int. Solid-State Circuits Conf.* (*ISSCC*), doi:10.1109/ISSCC.2012.6177086.

[14] Y. Park and D. D. Wentzloff, IR-UWB transmitters synthesized from standard digital library components, in *Proc. 2010 IEEE Int. Symp. Circuits and Systems*, Paris, France, 2010, pp. 3296–3299.

[15] L. Wang, Y. X. Guo, Y. Lian, and C. H. Heng, 3-to-5GHz 4-channel UWB beamforming transmitter with 1° phase resolution through calibrated vernier delay line in 0.13 μm CMOS, in *Proc. 2012 IEEE Int. Solid-State Circuits Conf.*, San Francisco, CA, USA, 2012, pp. 444–446.

[16] D. Lachartre, B. Denis, D. Morche, L. Ouvry, M. Pezzin, B. Piaget, J. Prouvee, and P. Vincent, A 1.1nJ/b 802.15.4a-compliant fully integrated UWB transceiver in 0.13 μm CMOS, in *Proc. 2009 IEEE Int. Solid-State Circuits Conf.–Digest of Technical Papers*, San Francisco, CA, USA, doi: 10.1109/ISSCC.2009.4977433.

[17] D. Liu, X. F. Liu, W. Rhee, and Z. H. Wang, A 7.6 mW 2 Gb/s proximity transmitter for smartphone-mirrored display applications, in *Proc. 2015 IEEE Asian Solid-State Circuits Conf.* (*A-SSCC*), Xiamen, China, 2015, pp. 1–4.

[18] N. Van Helleputte, M. Verhelst, W. Dehaene, and G. Gielen, A reconfigurable, 130 nm CMOS 108 pJ/pulse, fully integrated IR-UWB receiver for communication and precise ranging, *IEEE J. Solid-St. Circ.*, vol. 45, no. 1, pp. 69–83, 2010.

[19] D. Morche, G. Masson, S. De Rivaz, F. Dehmas, S. Paquelet, A. Bisiaux, O. Fourquin, J. Gaubert, and S. Bourdel, Double-quadrature UWB receiver for wide-range localization applications with sub-cm ranging precision, *IEEE J. Solid-St. Circ.*, vol. 48, no. 10, pp. 2351–2362, 2013.

[20] H. X. Song, D. Liu, W. Rhee, and Z. H. Wang, A 6–8 GHz 200 MHz bandwidth 9-channel VWB transceiver with 8 frequency-hopping subbands, in *Proc. 2018 IEEE Asian Solid-State Circuits Conf.* (*A-SSCC*), Tainan, China, 2018, pp. 295–298.

[21] J. F. M. Gerrits, H. Bonakdar, M. Detratti, E. Perez, M. Lobeira, Y. Zhao, Y. Dong, G. van Veenendaal, J. R. Long, J. R. Farserotu, et al., A 7.2–7.7 GHz FM-UWB transceiver prototype, in *Proc. 2009 IEEE Int. Conf. Ultra-Wideband*, Vancouver, Canada, 2009, pp. 580–585.

[22] N. Saputra and J. R. Long, A short-range low data-rate regenerative FM-UWB receiver, *IEEE Trans. Microw. Theory Tech.*, vol. 59, no. 4, pp. 1131–1140, 2011.

[23] Y. Z. Dong, Y. Zhao, J. F. M. Gerrits, G. van Veenendaal, and J. R. Long, A 9 mW high band FM-UWB receiver front-end, in *Proc. ESSCIRC 2008 – 34th European Solid-State Circuits Conf.*, Edinburgh, UK, 2008, pp. 302–305.

[24] F. Chen, W. Zhang, W. Rhee, J. Kim, D. Kim, and Z. H. Wang, A 3.8-mW 3.5–4-GHz regenerative FM-UWB receiver with enhanced linearity by utilizing a wideband LNA and dual bandpass filters, *IEEE Trans. Microw. Theory Tech.*, vol. 61, no. 9, pp. 3350–3359, 2013.

[25] D. Liu, X. H. Huang, Z. D. Ding, H. X. Song, W. Rhee, and Z. H. Wang, A 26.6 mW 1 Gb/s dual-antenna wideband receiver with auto beam steering for secure proximity communications, in *Proc. 2018 IEEE Custom Integrated Circuits Conf.* (*CICC*), San Diego, CA, USA, 2018, pp. 1–4.

[26] J. Ko and R. Gharpurey, A pulsed UWB transceiver in 65 nm CMOS with four-element beamforming for 1 Gbps meter-range WPAN applications, *IEEE J. Solid-St. Circ.*, vol. 51, no. 5, pp. 1177–1187, 2016.

[27] C. H. Hu, R. Khanna, J. Nejedlo, K. M. Hu, H. P. Liu, and P. Y. Chiang, A 90 nm-CMOS, 500 Mbps, 3–5 GHz fully-integrated IR-UWB transceiver with multipath equalization using pulse injection-locking for receiver phase synchronization, *IEEE J. Solid-St. Circ.*, vol. 46, no. 5, pp. 1076–1088, 2011.

[28] N. S. Kim and J. M. Rabaey, A high data-rate energy-efficient triple-channel UWB-based cognitive radio, *IEEE J. Solid-St. Circ.*, vol. 51, no. 4, pp. 809–820, 2016.

[29] G. Lee, J. Park, J. Jang, T. Jung, and T. W. Kim, An IR-UWB CMOS transceiver for high-data-rate, low-power, and short-range communication, *IEEE J. Solid-St. Circ.*, vol. 54, no. 8, pp. 2163–2174, 2019.

[30] H. X. Song, D. Liu, Y. N. Zhang, W. Rhee, and Z. H. Wang, A 6.5–8.1-GHz communication/ranging VWB transceiver for secure wireless connectivity with enhanced bandwidth efficiency and $\Delta\,\Sigma$ energy detection, *IEEE J. Solid-St. Circ.*, vol. 55, no. 2, pp. 219–232, 2020.

[31] H. X. Song, W. Rhee, and Z. H. Wang, A 6–8 GHz multichannel reconfigurable pulse-based transceiver with 3.5 ns processing latency and 1 cm ranging accuracy for secure wireless connectivity, in *Proc. 2020 IEEE Custom Integrated Circuits Conf.* (*CICC*), Boston, MA, USA, 2020, pp. 1–4.

[32] H. X. Song, Z. D. Ding, W. Rhee, and Z. H. Wang, A secure TOF-based transceiver with low latency and sub-cm ranging for mobile authentication applications, in *Proc. 2018 IEEE Radio Frequency Integrated Circuits Symp.* (*RFIC*), Philadelphia, PA, USA, 2018, pp. 160–163.

Bowen Wang received the BEng degree in integrated circuit design & integrated system from Xidian University, Xi'an, China in 2018. He is currently a PhD candidate in microelectronics at Tsinghua University, Beijing, China. His current research interests include all-digital phase-locked loop and low-power transceiver for short-range communications.

Haixin Song received the BEng degree in microelectronics from Tsinghua University, Beijing, China in 2015. He is currently a PhD candidate at Tsinghua University. His research interest includes analog and RF circuit design for low-power high-security transceiver systems.

Woogeun Rhee received the BEng degree in electronics engineering from Seoul National University, Seoul, Republic of Korea in 1991, the MEng degree in electrical engineering from the University of California, Los Angeles, USA in 1993, and the PhD degree in electrical and computer engineering from the University of Illinois, Urbana-Champaign, USA in 2001.

From 1997 to 2001, he was at Conexant Systems, Newport Beach, CA, USA, where he was a principal engineer and developed low-power and low-cost fractional-N synthesizers. From 2001 to 2006, he was at IBM Thomas J. Watson Research Center, Yorktown Heights, NY, USA, and worked on clocking area for high-speed I/O serial links, including low-jitter phase-locked loops, clock-and-data recovery circuits, and on-chip testability circuits. In August 2006, he joined the School of Integrated Circuits as an associate professor at the School of Integrated Circuits (formerly, the Institute of Microelectronics and the Department of Microelectronics and Nanoelectronics), Tsinghua University, Beijing, China, and became a professor in December 2011.

His current research interests include short-range low-power radios for next generation wireless systems and clock/frequency generation circuits for wireline and wireless communications.

He holds 24 U.S. patents. He is an ex-officio AdCom member (2020–2021) of the Solid-State Circuits Society and an IEEE Distinguished Lecturer (2016–2017). He currently serves as an associate editor for *IEEE Open Journal of the Solid-State Circuit Society*. He has been an associate editor for *IEEE Journal of Solid-State Circuits* (2012–2018), *IEEE Transactions on Circuits and Systems Part-II*: *Express Briefs* (2008–2009), and a guest editor for *IEEE Journal of Solid-State Circuits Special Issues* in November 2012 and November 2013. He has served on the technical program committees of several IEEE conferences, including ISSCC, CICC, and A-SSCC. He is the TPC chair of A-SSCC 2021.

Zhihua Wang received the BEng, MEng, and PhD degrees in electronic engineering from Tsinghua University, Beijing, China in 1983, 1985, and 1990, respectively. Since 1997, he has been a full professor at Tsinghua University. Since 2000, he has been the deputy director of the School of Integrated Circuits, Tsinghua University. From 1992 to 1993, he was a visiting scholar at CMU. He was a visiting scholar at KU Leuven from 1993 to 1994. From September 2014 to March 2015, he was a visiting professor at HKUST. He has coauthored 13 books/chapters, over 225 (569) articles in international journals (conferences), over 251 (29) articles in Chinese journals (conferences), and holds 130 Chinese and 10 U.S. patents. His current research mainly focuses on CMOS RFIC and biomedical applications, involving RFID, PLL, low-power wireless transceivers, and smart clinic equipment combined with leading edge RFIC and digital image processing techniques.

He was an AdCom member of the IEEE SSCS from 2016 to 2019. He was a Technology Program Committee member of the IEEE ISSCC from 2005 to 2011. Since 2005, he has been a steering committee member of the IEEE A-SSCC. He has served as the chairman of IEEE SSCS Beijing Chapter from 1999 to 2009. He was the technical program chair for A-SSCC 2013. He was a guest editor for *IEEE Journal of Solid-State Circuits* (*JSSC*) special issues in December 2006, December 2009, and November 2014. During 2019–2020, he has been an associate editor in chief of *IEEE Open Journal of Circuits and Systems*. He had been an associate editor of *IEEE Transactions On Circuits And Systems—I*: *Regular Papers* during 2016–2019, *IEEE Transactions on Circuits and Systems—II*: *Express Briefs* during 2010–2013, *IEEE Transactions on Biomedical Circuits and Systems* (*BioCAS*) during 2008–2015, and other administrative/expert committee positions in China's national science and technology projects. From 2018 to 2019, he was an IEEE SSCS distinguished lecturer. Since 2020, he has been an IEEE CASS distinguished lecturer.